Tellus (2002), 54A, 390–405
Printed in UK. All rights reserved

TELLUS
ISSN 0280–6495

Significance of non-rotational wind stress in the seasonal variation of continental torque

By MAYUMI K. YOSHIOKA*, HIROSHI NIINO and RYUJI KIMURA, *Ocean Research Institute, University of Tokyo, 1-15-1 Nakano-ku, Minamidai, Tokyo, 164-8639, Japan*

(Manuscript received 30 August 1999; in final form 22 February 2002)

ABSTRACT

The physical mechanism by which seasonally varying atmospheric wind stress exerted on the sea surface is communicated to the solid earth as oceanic pressure torque (continental torque) and bottom frictional torque is investigated with a linear shallow-water numerical model of barotropic oceans. The model has a realistic land–ocean distribution and is driven by a seasonally varying climatic wind stress. A novel way to decompose the wind stress into rotational and non-rotational components is devised. The rotational component drives ocean circulations as classical theories of wind-driven circulations demonstrate. The non-rotational component does not produce ocean circulations within the framework of a barotropic shallow-water model, but balances with the pressure gradient force due to surface displacement in the steady state. Based on this decomposition, it is shown that most of the continental torque which plays a major role in producing the seasonal variation of length of day (LOD) is caused by the non-rotational component of the wind stress. Both continental torque due to the wind-driven circulation produced by the rotational component of the wind stress and the bottom frictional torque are of minor importance.

1. Introduction

The seasonal variation of length of day (LOD) is explained by the variation of the atmospheric angular momentum, because the sum of the angular momenta of the atmosphere and of the solid earth is almost conserved (e.g. Rosen et al., 1990). The angular momentum is transferred within a few days from the atmosphere to the solid earth, and the seasonal variation of the total oceanic angular momentum is generally small in comparison with that of the atmospheric angular momentum (Munk and MacDonald, 1960). The oceans, which cover nearly 70 % of the earth's surface, however, work as an important conveyor of the angular momentum between the atmosphere and the solid earth (Ponte, 1990).

*Corresponding author.
e-mail: yoshioka@ori.u-tokyo.ac.jp

At the land surface, the angular momentum of the atmosphere is transferred directly to the solid earth through pressure torque (so-called mountain torque) and frictional torque. Over the oceans, on the other hand, it is transferred in a more indirect manner: the wind drives oceanic motions, which, in turn, generate frictional torque at the bottom of the ocean. It also produces a certain pressure distribution at the boundaries of the oceans and exerts so-called 'continental torque' on the solid earth.

Using a numerical model of an ocean circulation driven by time-varying zonal wind stress, Ponte (1990) examined the role of the oceanic torques in the transfer of the angular momentum. His model ocean was a rectangle, the boundaries of which consist of latitudinal and longitudinal lines. He found that the wind stress torque at the ocean surface nearly coincides with the continental torque and that the bottom frictional torque is negligibly small. He also suggested that the barotropic response is important for the rapid transfer of angular momentum via the ocean. He concluded that the ocean works as a conveyor of angular momentum between the atmosphere and the solid earth. Ponte and Gutzler (1991) used a numerical model similar to the one by Ponte (1990) and studied the angular momentum balance associated with the Madden–Julian oscillation (MJO) over the tropical Pacific ocean. They found that the wind stress torque over the ocean nearly balances with the continental torque, and this balance is established rapidly through the barotropic process.

These previous studies revealed that the barotropic response of the oceans to the seasonal variation of the wind stress is important for the rapid transfer of the angular momentum from the atmosphere to the solid earth via the oceans. Furthermore, the continental torque caused by the sea surface displacement is the main process to transfer the angular momentum between them (Oort 1985; 1989; Oort and Peixoto 1992). However, the physical mechanism by which the wind stress causes the continental torque does not seem to have been examined in detail.

Ponte and Rosen (1994) investigated the role of the bottom pressure torque based on the sea surface displacement estimated from the geostrophic currents. This may seem to be plausible, because the large-scale atmospheric flow is quasi-geostrophic and mainly rotational. Thus, the surface wind stress has non-vanishing curl and produces wind-driven circulations. However, even if the wind over the ocean is purely geostrophic, observed wind field contains a component which is not used to create the wind-driven circulation[1], because the ocean is confined in a closed basin. This fact may be visualized if one recalls that the structure of a wind-driven circulation is mathematically obtained by solving the vorticity equation which contains only the stress curl of wind fields. This means that there are many different wind fields which yield the same wind-driven circulation. When we would like to obtain the continental torque, however, not only the wind stress curl but also the wind field itself over the ocean becomes crucial. Part of the wind field drives ocean circulations which may cause continental torque through the sea surface displacements, while the rest (which has no stress curl) causes the continental torque without the ocean circulation.

Using a steady linear barotropic ocean model with a flat bottom on a beta plane (e.g. Stommel, 1948), Masuda (1991) suggested that the net pressure force at the eastern and western boundaries of an ocean basin does not depend on the ocean circulation and is determined solely by the total wind stress exerted on the ocean surface. In other words, the whole ocean behaves as if it were a flat land, as far as the zonal force exerted on the solid earth is concerned.

He also suggested that the sea surface displacement caused by the wind-driven circulation is not important for creating the continental torque. If this is true, it should be possible to extract from the observed wind fields a wind component that does not produce the wind-driven circulation but does cause the continental torque. This possibility motivated us to investigate how the wind-driven circulation contributes to the continental torque and the resulting seasonal variation of the LOD by means of a linear barotropic numerical model of the 'quasi-global' wind-driven circulation in a spherical coordinate.

The numerical model used in the present study is called 'quasi-global' because it does not contain the bottom topography and the Antarctic Circumpolar Current (ACC). Although we are aware that the inclusion of them is indispensable to make a quantitative estimate of the contribution of the oceanic wind stress to the seasonal variation of the LOD, our main interest here is to clarify the basic dynamical process to produce the continental torque in the mid- and low-latitude oceans from the wind stress. We will exclude the ACC in our model, since it is not possible to reproduce a realistic ACC in a barotropic shallow-water model without bottom topography.

In the next section, briefly reviewed is the relationship between the wind stress and the pressure force exerted on an ocean basin for a steady-state wind-driven circulation on a beta plane, which helps us to consider the mechanism of the

[1] This statement is correct only for a barotropic shallow-water ocean model which does not consider the surface Ekman layer explicitly. If a barotropic model with the surface Ekman layer is considered, a wind stress with no stress curl does cause an interior geostrophic flow to compensate the Ekman layer flow (Pedlosky, 1968; Veronis, 1996). The pressure distribution balanced with the geostrophic flow, however, is shown to be the same as that obtained from the shallow-water barotropic model.

torque balance in the realistic oceans. In Section 3, a linear numerical model of the global barotropic oceans which are driven by the observed wind stress is described. The results are presented in Section 4. The wind stress is decomposed into the rotational and non-rotational components and contribution of each component to the continental torque is examined. The results are discussed in Section 5 and conclusions are given in Section 6.

2. Torque balance for steady motions on a beta-plane

For steady motions of a barotropic ocean on a beta plane, there exists a simple relationship between the pressure force exerted on the ocean basin and the surface wind stress, provided that the bottom frictional force is a linear function of the flow velocity (Masuda, 1991)[2]. It holds for an ocean of an arbitrary shape with an arbitrary wind stress distribution on a beta plane.

The basic linear equations in the steady state may be written as

$$f(y)\boldsymbol{k}\times\boldsymbol{v} = -\nabla p - R\boldsymbol{v} + \boldsymbol{\tau}(x, y) \tag{1}$$

and

$$\nabla\cdot\boldsymbol{v} = 0, \tag{2}$$

where $\boldsymbol{v}$ is the current velocity, p the pressure, $\boldsymbol{k}$ the unit vector in the z-direction (upward), R the coefficient of the bottom friction which is proportional to $\boldsymbol{v}$, $f(y)$ the Coriolis parameter as a function of y (meridional direction) and $\boldsymbol{\tau} = (\tau_x, \tau_y)$ the wind stress vector at the sea surface. The net pressure force in the x-direction (eastward) exerted on the ocean basin is expressed as

$$F_x = \oint_L p\boldsymbol{i}\cdot \mathrm{d}\boldsymbol{l} = \int_S \frac{\partial p}{\partial x}\,\mathrm{d}x\,\mathrm{d}y, \tag{3}$$

where $\boldsymbol{i}$ is the unit vector in the x-direction and $\mathrm{d}\boldsymbol{l}$ the line element vector along the coasts. L and S denote the whole length of the coasts and the whole area of the ocean basin, respectively. Substituting $\partial p/\partial x$ from the x-component of Eq. (1) into Eq. (3) and using the continuity equation (2), we obtain

$$F_x = \int_S \tau_x(x, y)\,\mathrm{d}x\,\mathrm{d}y. \tag{4}$$

Equation (4) states that the net zonal pressure force exerted on the ocean basin on the beta plane is determined solely by the area integral of the x-component of the surface wind stress $\tau_x(x, y)$ (Masuda, 1991; 1998). It does not depend on the wind-driven circulation, although the meridional distribution of the zonal pressure force along the coast depends strongly on it.

To obtain more insight into what the relationship means physically, let us now divide $\boldsymbol{\tau}(x, y)$ into two parts as

$$\boldsymbol{\tau}(x, y) = \boldsymbol{\tau}^{\mathrm{R}} + \boldsymbol{\tau}^{\mathrm{NR}} = \boldsymbol{k}\times\nabla\psi_\tau(x, y) + \nabla\phi_\tau(x, y), \tag{5}$$

where the first term in the right-hand side denotes the 'rotational' component of the wind stress $\boldsymbol{\tau}^{\mathrm{R}}$ and the second term the 'non-rotational' component $\boldsymbol{\tau}^{\mathrm{NR}}$, respectively (for simplicity, $\boldsymbol{\tau}$, $\boldsymbol{\tau}^{\mathrm{R}}$ and $\boldsymbol{\tau}^{\mathrm{NR}}$ will be hereafter referred to as total, rotational and non-rotational wind stresses, respectively).

The way to decompose $\boldsymbol{\tau}$ into $\boldsymbol{\tau}^{\mathrm{R}}$ and $\boldsymbol{\tau}^{\mathrm{NR}}$ for a given observed wind field depends upon the boundary conditions for ψ_τ and ϕ_τ at the coastlines. It looks apparent at the first sight that the zonal wind with meridional shear belongs to the rotational wind. However, if we recall that the regional integral of the curl of the wind stress field at the sea surface is equal to the circulation along the closed coastline, we realize that the normal component of the wind at the coastline does not contribute to the circulation. This fact suggests that one should divide the wind stress into the two components, so that the non-rotational wind stress has only the normal component to the coastline and the rotational wind stress the alongshore component of the wind field[3]. The pressure forces resulting from $\boldsymbol{\tau}^{\mathrm{R}}$ and $\boldsymbol{\tau}^{\mathrm{NR}}$ are similarly

[2] Masuda (1991) derived this relationship for linear steady motions. However, it can be generalized to nonlinear steady motions for which Eq. (1) is replaced by

$$(\boldsymbol{v}\cdot\nabla)\boldsymbol{v} + f(y)\boldsymbol{k}\times\boldsymbol{v} = -\nabla p - R\boldsymbol{v} + \boldsymbol{\tau}(x, y),$$

(Masuda, personal communication, 1998).

[3] This decomposition produces τ_y even when the 'original' wind stress is purely zonal. By introducing τ_y, which does not come into the angular momentum balance at all, however, it becomes possible to decompose the original wind stress into rotational and non-rotational components which contribute to a better understanding of the momentum transfer process between the atmosphere and the solid earth through the oceans.

denoted by F_x^{R} and F_x^{NR}, respectively. Since τ_x^{R} is written as

$$\tau_x^{\mathrm{R}} = -\frac{\partial \psi_\tau}{\partial y}, \tag{6}$$

substitution of Eq. (6) into Eq. (4) leads to

$$F_x^{\mathrm{R}} = 0. \tag{7}$$

Thus, the rotational wind stress which causes the wind-driven circulation produces no net zonal pressure force on the beta plane.

For a general distribution of the wind stress, however, the non-rotational wind stress which does not vanish when integrated in the meridional direction would produce a net pressure force. Furthermore, Eq. (7) does not hold strictly on a spherical coordinate system, and an analogue of Eq. (7) does not hold for the continental torque of oceans on the globe because the arm length from the rotation axis varies with latitude. Thus, there is a possibility that the rotational wind stress produces some continental torque in the real oceans. It then becomes important to know the magnitudes of the rotational and non-rotational wind stresses for the real oceans, and to know which stress contributes more to the continental torque. To answer these questions, we have performed a numerical simulation of the quasi-global ocean circulation driven by the observed climatic wind stress.

3. Numerical model

A linear barotropic model of a quasi-global ocean circulation driven by the observed climatic wind stress is used in this study. The governing equations are linearized shallow water equations in the spherical coordinate:

$$\frac{\partial u}{\partial t} - fv = -\frac{g}{a\cos\phi}\frac{\partial \eta}{\partial \lambda} + \frac{\tau_\lambda}{D\rho} - Ru, \tag{8}$$

$$\frac{\partial v}{\partial t} + fu = -\frac{g}{a}\frac{\partial \eta}{\partial \phi} + \frac{\tau_\phi}{D\rho} - Rv, \tag{9}$$

$$\frac{\partial \eta}{\partial t} + D\left(\frac{1}{a\cos\phi}\frac{\partial u}{\partial \lambda} + \frac{1}{a\cos\phi}\frac{\partial (v\cos\phi)}{\partial \phi}\right) = 0, \tag{10}$$

where u and v are the zonal and meridional velocity components of the oceanic current, respectively. η is the sea surface displacement from the initial state of the rest. τ_λ and τ_ϕ are the zonal and meridional components of the wind stress, respectively. λ is longitude, ϕ latitude, g the acceleration of gravity, a the mean radius of the earth, D the constant ocean depth, ρ the density of water, f the Coriolis parameter, and R a linear bottom frictional coefficient.

The model ocean in this study has $R^{-1} = 5$ d and a constant depth of D ($= 4000$ m), and is confined to the latitudinal range between 57.5°S and 67.5°N. In the present calculation, the ACC is excluded[4]. The spatial derivatives are approximated by the central differences scheme with a staggered grid configuration, where the horizontal resolution is 2.5° × 2.5° (Fig. 1). The zonal boundaries of the oceans for each latitude are given from the Land and Ocean Distribution Data provided by Oki (1991, personal communication). The free slip condition with no normal flow is imposed at the boundaries.

The monthly wind stress data based on observations from 1879 to 1976 (Hellerman and Rosenstein, 1982) are used to drive the ocean circulation. The original data cover the whole globe with 1° × 1° mesh. The wind stress, $\boldsymbol{\tau} = (\tau_\lambda, \tau_\phi)$ for each time step was calculated by a linear interpolation of the monthly data. τ_λ and τ_ϕ are imposed at the same grid point as u and v, respectively (Fig. 1). The wind stress at the coastline, however, was set to be equal to zero. Time integration was done with the leap-frog scheme with a time step of 3 min, except that the Matsuno scheme was used for every 20 time steps.

Time rate of change of the total oceanic angular momentum M_{o} about the polar axis is expressed as

$$\frac{\mathrm{d}M_{\mathrm{o}}}{\mathrm{d}t} = T_{\mathrm{w}} - T_{\mathrm{c}} - T_{\mathrm{b}}, \tag{11}$$

where

$$T_{\mathrm{w}} = \int_\phi \int_\lambda \tau_\lambda(\lambda, \phi)(a\cos\phi)\,\mathrm{d}A, \tag{12}$$

[4] The current assessment of the role of the ACC on the seasonally varying oceanic torque balance seems to be rather controversial. Ponte and Rosen (1993) estimated the bottom pressure torque around the ACC at Drake Passage and concluded that its contribution to the oceanic torque balance is small. Bryan (1997) found that there is a remarkable seasonal variation of oceanic angular momentum around the ACC latitudes, but did not examine seasonal variation of the oceanic torque balance.

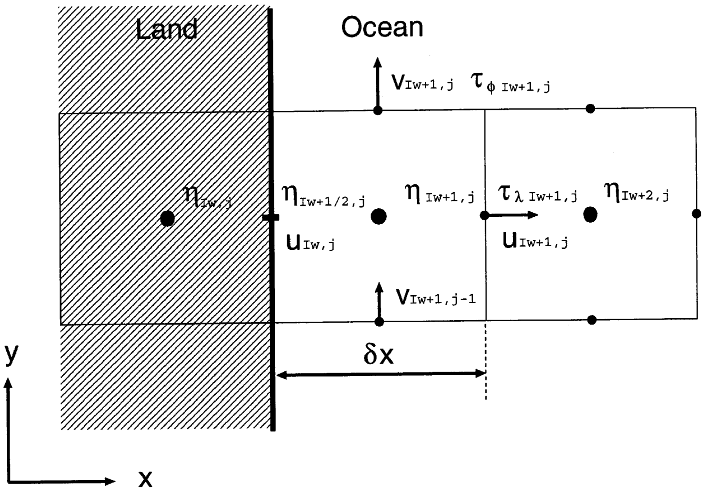

Fig. 1. The horizontal grid configuration in the western boundary region.

$$T_c = -\rho g D \int_\phi \int_\lambda \frac{\partial \eta(\lambda, \phi)}{\partial \lambda} \, dA, \tag{13}$$

$$T_b = -R\rho D \int_\phi \int_\lambda u(\lambda, \phi)(a \cos \phi) \, dA, \tag{14}$$

are the the wind stress torque at the ocean surface, the continental torque and the bottom frictional torque, respectively (Ponte, 1990; Ponte and Gutzler, 1991; see also Appendix A). $dA = a \cos \phi \, d\lambda \, a \, d\phi$ and the integrals in Eqs. (12)–(14) are taken over the whole oceans. The eastward torque is taken positive. Equation (11) states that the time rate of change of the angular momentum is equal to the sum of external torques. As is described in detail in Appendix A, our finite-difference schemes exactly conserve the oceanic angular momentum in the absence of the external torques. The continental torque (13) has been also calculated in a way consistent with the angular momentum conservation and the boundary conditions (see Appendix A).

When one considers the seasonal variation of LOD, it is known that dM_o/dt is generally small in comparison with the variation of the atmospheric angular momentum (Munk and MacDonald, 1960). Therefore, the three terms in the right-hand side of Eq. (11) are nearly in balance: i.e.,

$$0 \simeq T_w - T_c - T_b. \tag{15}$$

4. Results

4.1. *Seasonal variation of the wind driven circulation*

The time integration was started from the state of rest and was carried out for 2 yr. The spin-up was completed within the first 5 d ($\sim R^{-1}$), and thereafter a regular seasonal change was obtained. Figure 2(a) shows the annually averaged sea surface displacement $\bar{\eta}$ caused by the annually averaged total wind stress $\bar{\boldsymbol{\tau}}$, where the overbar denotes the annual average. In the Kuroshio region, the maximum sea surface displacement reaches about 6 cm. The volume transport estimated from the geostrophic relation ($fv = g\Delta\eta/\Delta x$) is about 32 Sv ($= 32 \times 10^6$ m^3 s^{-1}). This value is somewhat smaller than the observed volume transport of about 50 Sv in the Kuroshio region (Ichikawa and Beardsley, 1993). As far as the volume transport is concerned, our model simulates reasonably well the gyres of the real oceans. The simulated characteristic velocity of the Kuroshio, on the other hand, is 2.2 cm s^{-1}, which is much smaller than the observed value of 30 cm s^{-1}. This discrepancy is mainly caused by our assumption of the barotropic ocean with the depth of 4000 m.

4.2. *Seasonal variation of oceanic torque*

Figure 3(a) shows the seasonal variations of the wind stress torque T_w, continental torque T_c and

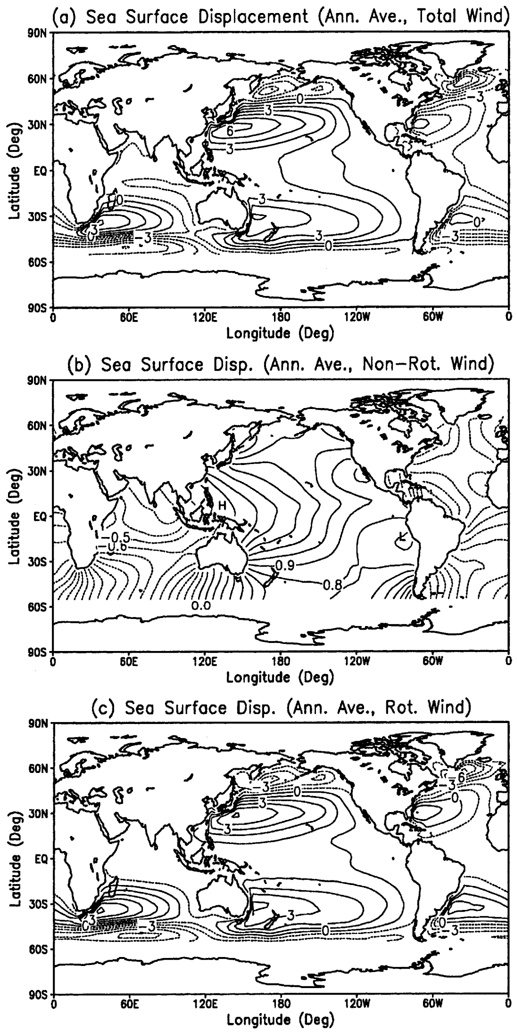

Fig. 2. Sea surface displacement caused by the annually averaged wind of Hellerman and Rosenstein (1983) for (a) total wind stress, (b) non-rotational wind stress and (c) rotational wind stress, respectively. The contour interval is 1 cm for (a) and (c), and 0.1 cm for (b).

bottom frictional torque T_b. The variation of T_c nearly coincides with that of T_w, indicating that most of the seasonally varying wind stress torque exerted on the ocean surface is given to the solid earth as the continental torque. The fact that there is little time lag between T_w and T_c suggests that the transfer of the angular momentum occurs very quickly from the atmosphere to the solid earth through the oceans: i.e., the angular momentum of the ocean, M_o, experiences very little seasonal variation. These results are consistent with the previous studies (Ponte, 1990; Ponte and Gutzler, 1991; Rosen et al., 1990).

Figure 3(a) also shows that the amplitudes of the seasonal variations of T_w and T_c are about 7 HU (1 Hadley Unit = 10^{18} N m). Wahr and Oort (1984) estimated the total required torque and the mountain torque from observational data. Considering that the land torque shows a seasonal variation similar to that of the mountain torque except that the amplitude is a factor of 2 or 3 larger (e.g., Boer, 1990), the amplitude of the seasonal variations of T_w in the present simulation seems to be nearly comparable to the results by Wahr and Oort (1984). Maxima of T_c and T_w causing an acceleration of the earth's rotation occur in June, while their minima causing a deceleration occur in April.

In contrast to T_c, the bottom frictional torque T_b plays a minor role in transferring angular momentum through the oceans, as was pointed out by Ponte (1990) and Ponte and Gutzler (1991).

4.3. Oceanic response to non-rotational and rotational wind stress

There are two mechanisms which produce the sea surface displacements. In the steady state, the non-rotational wind stress $\boldsymbol{\tau}^{NR}$ balances with the pressure gradient force due to the sea surface slope[5]. The other is the sea surface displacement caused by the ocean circulations, which are driven solely by the rotational wind stress $\boldsymbol{\tau}^{R}$. Thus, by dividing the total wind stress $\boldsymbol{\tau}$ into $\boldsymbol{\tau}^{R}$ and $\boldsymbol{\tau}^{NR}$, one can study the mechanism by which the oceanic torques are produced from the wind stress torque. A detailed description of the method to decompose $\boldsymbol{\tau}$ into $\boldsymbol{\tau}^{R}$ and $\boldsymbol{\tau}^{NR}$ is given in Appendix B.

Figure 4 shows the magnitude of the annually averaged rotational and non-rotational wind stress $\bar{\tau}_\lambda^{R}$ and $\bar{\tau}_\lambda^{NR}$, respectively. It is seen that the rotational wind stress $\bar{\tau}_\lambda^{R}$ [Fig. 4(b)] has a larger

[5] Strictly speaking, purely zonal wind stress with zero stress curl produces a geostrophic meridional flow that compensates the meridional transport in the surface Ekman layer and balances with the sea surface slope (Veronis, 1996). A calculation shows, however, that this effect causes exactly the same sea surface slope as that caused by the simple wind drift in the shallow-water model.

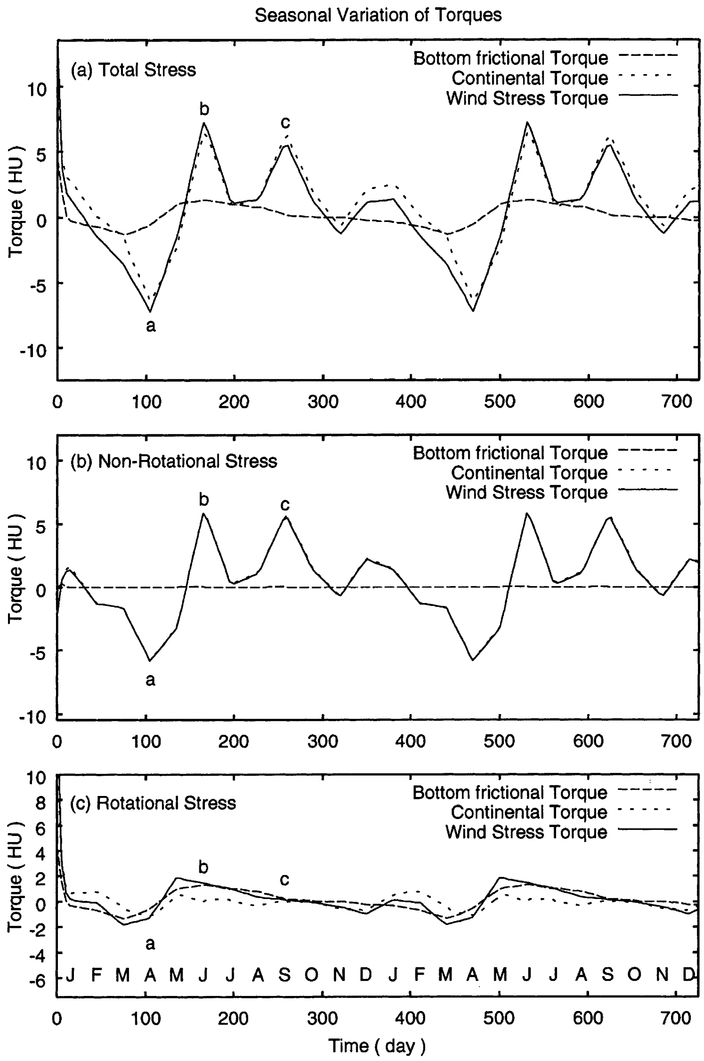

Fig. 3. Seasonal variations of the simulated torques for (a) the original wind stress data by Hellerman and Rosenstein (1983), (b) non-rotational wind stress and (c) rotational wind stress, respectively. The ordinate is Julian for days starting from 1 January. The results are shown for 2 yr (730 d). The abscissa is the torque which is taken positive to the east. The thick line is the wind stress torque T_w from the atmosphere to the oceans, the dotted line the continental torque T_c, and the dashed line the bottom frictional torque T_b due to the ocean current.

amplitude near the center of the oceans, while that the non-rotational wind stress $\bar{\tau}_\lambda^{NR}$ near the boundaries of the oceans [Fig. 4(a)]. A pair of positive and negative peaks of $\bar{\tau}_\lambda^{R}$ in each ocean corresponds to an oceanic gyre.

Figure 5 shows the annually-averaged total, non-rotational and rotational wind stress vectors. Both of the Pacific and Atlantic oceans have anticyclonic circulation patterns of rotational wind stress vector in the Northern and Southern Hemispheres, respectively, while the Indian ocean has one anticyclonic circulation pattern [Fig. 5(b)]. The non-rotational wind stress vector [Fig. 5(c)] is obtained by subtracting the rotational wind stress from the total wind stress [Fig. 5(a)]. In the Pacific and Atlantic oceans in

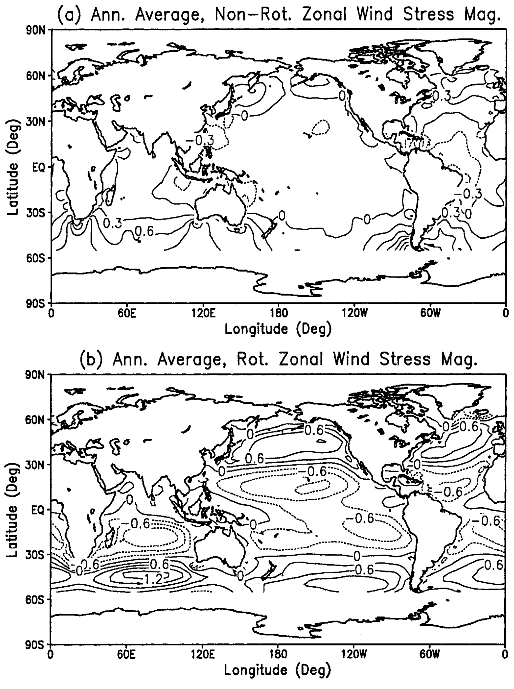

Fig. 4. Global distribution of the magnitude of the zonal wind stress. (a) non-rotational and (b) rotational components of the wind stress. The contour interval is 0.3 dyn cm^{-2}.

the Northern Hemisphere, the non-rotational wind stress vector is southwestward on the northwest coast and is eastward on the northeast coast. It is westward near the equator. In the Southern Hemisphere, the non-rotational wind stress vector shows cyclonic circulation patterns around the southern edges of Africa and Australia continents. A part of these circulation patterns are caused to compensate the anticyclonic circulation patterns due to the rotational wind stress. Another cyclonic circulation pattern seems to exist around the southern edge of the South America at a first sight. Since the Drake passage is closed in the present model, however, the wind vector is not continuous across the South America continent.

Figures 2(b) and (c) show annually averaged sea surface displacements $\bar{\eta}^{\mathrm{NR}}$ and $\bar{\eta}^{\mathrm{R}}$ produced by $\bar{\boldsymbol{\tau}}^{\mathrm{NR}}$ and $\bar{\boldsymbol{\tau}}^{\mathrm{R}}$, respectively, where two separate runs were made to obtain these displacements. Since our model is linear, a superposition of Figs. 2(b) and (c) yields exactly the same pattern as Fig. 2(a). It is seen that the maximum of $\bar{\eta}^{\mathrm{R}}$ is about three

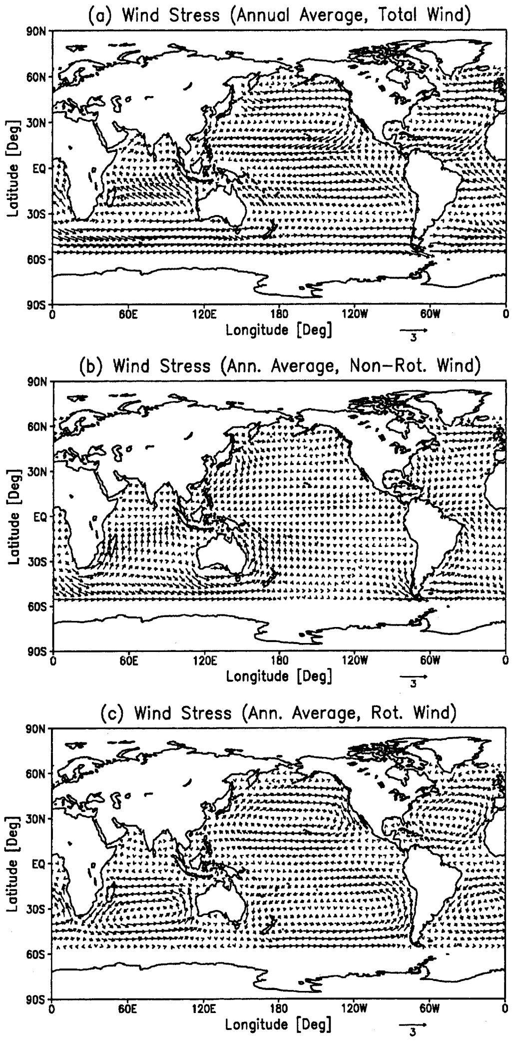

Fig. 5. Annually averaged (a) total wind stress, (b) non-rotational wind stress and (c) rotational wind stress vectors. The wind stress data by Hellerman and Rosenstein (1983) have been used for the calculation. The arrow in the lower-right of each figure corresponds to 3 dyn cm^{-2}.

times larger than that of $\bar{\eta}^{\mathrm{NR}}$. Therefore, the pattern of Fig. 2(c) is rather similar to that of Fig. 2(a) : i.e., the annually averaged circulation is mainly produced by $\bar{\boldsymbol{\tau}}^{\mathrm{R}}$. Note that $\bar{\eta}^{\mathrm{R}}$ is proportional to the stream function except near the equator. For the non-rotational wind stress, the horizontal pressure gradient force balances with the wind stress in the steady state. Since the zonal wind is predominant in the annual average, the ocean surface generally slopes to the east–west direction as shown in Fig. 2(b). Such a force balance is also observed around the southern ends of Africa and Australia, where the non-rotational surface elevation generally increases anticlockwise. Near the southern end of South America, the non-rotational surface elevation reaches a maximum on its west coast and a minimum on its east coast.

The annually averaged surface displacement and wind stress vector are shown above in order to illustrate how the suggested decomposition looks like. It is important to note that, although the rotational component has a large amplitude near the center of oceans, its amplitude near the coast remains considerably small. The non-rotational component, on the other hand, has a relatively large amplitude even near the coast. As will be demonstrated below, these properties of rotational and non-rotational components becomes more important when the seasonal variation of the torques are considered.

4.4. *Torques produced by non-rotational and rotational wind stress*

Figure 3(b) shows the seasonal variations of torques T_w^{NR}, T_c^{NR} and T_b^{NR} produced by the non-rotational wind stress $\boldsymbol{\tau}^{NR}$. The seasonal variation of T_w^{NR} shows a remarkable similarity to that of T_w in Fig. 3(a), suggesting that a major part of T_w consists of T_w^{NR}. Furthermore, Fig. 3 (b) shows that almost all T_w^{NR} is converted into the non-rotational continental torque, T_c^{NR}. Accordingly, the total continental torque T_c in Fig. 3(a) nearly coincides with T_c^{NR}. T_b^{NR} is negligibly small in seasonal variation, because $\boldsymbol{\tau}^{NR}$ balances quickly with the pressure gradient force without leaving noticeable circulations.

Figure 3(c) shows the seasonal variations of the oceanic torques T_w^R, T_c^R and T_b^R produced by the rotational wind stress $\boldsymbol{\tau}^R$. Since the bottom frictional torque is only produced by $\boldsymbol{\tau}^R$, T_b^R coincides with T_b in Fig. 3(a). The continental torque T_c^R produced by $\boldsymbol{\tau}^R$ is of the same order of T_b^R, and is much smaller than T_c^{NR} in Fig. 3(b). The presence of T_c^R, however, demonstrates that the relationship (7) on the beta plane does not strictly hold for the real oceans with sphericity.

4.5. *Meridional distribution of oceanic torques*

Figures 6(a), (b) and (c) show time–latitude cross-sections of seasonally varying $T_w(\phi)$, $T_c(\phi)$ and $T_b(\phi)$, respectively, where $T_w(\phi)$, for example, is defined by $\int_\lambda T_w a^2 \cos^2 \phi \, d\lambda \, a\Delta\phi$, at each latitudinal grid point. $\Delta\phi$ is the latitudinal grid interval of 2.5°. $T_w(\phi)$ has peaks of its amplitudes at the latitudes around 10° and 35° in both Hemispheres and around 50°S. Although variations of the displacement around these low latitudes have relatively small amplitude (not shown), the long arm length from the rotation axis near the equator causes significant amplitude of the variation of the torques.

The latitudinal distributions of both $T_c(\phi)$ and $T_b(\phi)$ show somewhat similar pattern to that of $T_w(\phi)$, implying that there is little meridional redistribution of the atmospheric angular momentum through the torques in the ocean. In the Southern Hemisphere the magnitude of $T_c(\phi)$ is nearly of the same order as that of $T_b(\phi)$. In the Northern Hemisphere, on the other hand, the magnitude of $T_c(\phi)$ is greater than that of $T_b(\phi)$. These features are commonly found in all months.

In mid-latitudes of the Northern Hemisphere around 35°N, the largest amplitude of $T_w(\phi)$ and $T_c(\phi)$ are found in winter (January and February around day 360). $T_b(\phi)$ has a weak peak at around 35°N and has another peak in the amplitude at around 50°S latitudinal belt where the amplitudes of $T_w(\phi)$ and $T_c(\phi)$ are small.

The amplitude of the seasonal variation of $T_c(\phi)$ is only about 1.5–2 times larger than that of $T_b(\phi)$ at most latitudes. It is interesting to note that once they are integrated meridionally, however, the continental torque becomes much larger than the bottom frictional torque [Fig. 3(a)].

Now we examine contributions of the rotational and non-rotational wind stress torques to the oceanic torques. Figure 6(d) shows the time-latitude cross section of the non-rotational wind stress torque $T_w^{NR}(\phi)$. $T_c^{NR}(\phi)$ is not shown here, since its latitudinal pattern is nearly the same as $T_w^{NR}(\phi)$. $T_b^{NR}(\phi)$ is not shown since it is negligibly small everywhere. Figures 6 (e) and (f) show the wind stress torque and continental torque caused by the rotational wind stress $T_w^R(\phi)$ and $T_c^R(\phi)$, respectively. The amplitude of seasonal variation of $T_w^{NR}(\phi)$ is roughly a half of that of $T_w^R(\phi)$. Nevertheless the amplitude of $T_c^{NR}(\phi)$ is about

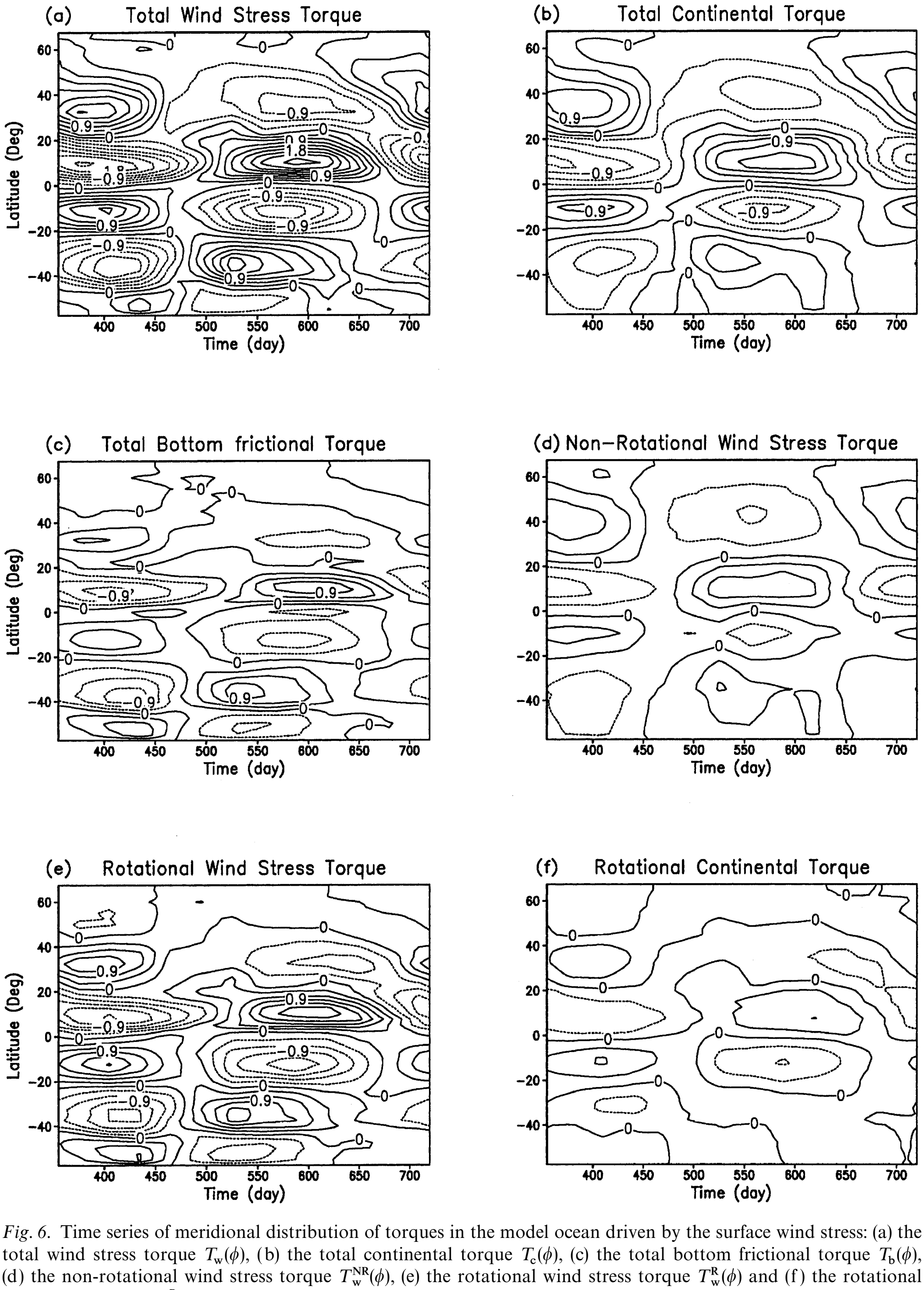

Fig. 6. Time series of meridional distribution of torques in the model ocean driven by the surface wind stress: (a) the total wind stress torque $T_w(\phi)$, (b) the total continental torque $T_c(\phi)$, (c) the total bottom frictional torque $T_b(\phi)$, (d) the non-rotational wind stress torque $T_w^{NR}(\phi)$, (e) the rotational wind stress torque $T_w^{R}(\phi)$ and (f) the rotational continental torque $T_c^{R}(\phi)$. The abscissa is latitude from 57.5°S to 67.5°N, and the ordinate Julian days. The contour interval is 0.3 HU. Solid lines denote positive values, while dashed lines denote negative values.

twice as large as that of $T_c^R(\phi)$: i.e., $T_c^{NR}(\phi)$ explains about two thirds of $T_c(\phi)$. $T_b^R(\phi)$ is not shown here because it is exactly the same as $T_b(\phi)$ shown in Fig. 6(c) (Note that T_b is produced by only the rotational wind stress.)

About two thirds of $T_w^R(\phi)$ is converted into $T_b^R(\phi)$ [Figs. 6(c) and (e)], while the rest into $T_c^R(\phi)$. Thus, $T_b^R(\phi)$ is larger than $T_c^R(\phi)$ in each latitudinal belt.

The contour patterns of the torques in Fig. 6 show no significant meridional phase shift. This again suggests that meridional redistribution of the angular momentum by the ocean circulation is of minor importance. Furthermore, the contour patterns show no time lag between the wind stress torques and the continental/bottom frictional torques.

5. Discussion

5.1. *Mechanism of angular momentum transfer via oceans*

It has been known that the continental torque is the dominant process in transferring atmospheric angular momentum to the solid earth through the oceans, thereby contributing to seasonal variation of the LOD (Ponte, 1990; Ponte and Gutzler, 1991; Ponte and Rosen, 1994). However, the mechanism by which the continental torque is produced by the wind stress torque has not been clarified previously. Using a linear barotropic quasi-global ocean circulation model which has a realistic land-ocean distribution and is driven by the observed wind stress distribution (Hellerman and Rosenstein, 1983), we have confirmed that the wind stress torque is mostly converted into the continental torque. Then the mechanism by which the continental torque is produced has been examined.

As was demonstrated in Section 2, it is known that for a barotropic ocean on a beta plane, the net pressure force in the x-direction is solely determined by the area integral of the wind stress in the x-direction and does not depend on the ocean circulation. This force balance holds for steady-state oceans on the beta plane but not for the torque balance in the real oceans for which the arm length from the rotation axis changes with latitude. Our results have shown, however, that the relationship similar to the force balance on the beta plane almost holds for the torque balance in the real oceans: If the wind stress is divided into the rotational and non-rotational components, the globally integrated continental torque is mostly caused by the non-rotational wind stress, and is contributed little by the ocean circulation driven by the rotational wind stress.

Based on the decomposition of the wind stress into the rotational and non-rotational components, the mechanism of the angular momentum transfer from the atmosphere to the solid earth via oceans may be considered in the following way. Firstly, although Figs. 6(a) and (e) show that the seasonally varying amplitude of $T_w^R(\phi)$ at each latitude is about two times larger than that of $T_w^{NR}(\phi)$, Fig. 3 shows that meridionally integrated T_w^R is much smaller than meridionally integrated T_w^{NR}. T_w^R is defined by

$$\begin{aligned} T_w^R &= \int_\phi T_w^R(\phi)\, d\phi \\ &= \int_\lambda \int_\phi \tau_\lambda^R a \cos\phi\, dA \\ &= -\int_\lambda \int_\phi \frac{1}{a} \frac{\partial \Psi_\tau}{\partial \phi} a^3 \cos^2\phi\, d\lambda\, d\phi \end{aligned} \tag{16}$$

[see Eq. (38) in Appendix B]. If the $\cos^2\phi$ term were absent, T_w^R would vanish because of the boundary conditions for Ψ_τ. Since $\partial\Psi_\tau/\partial\phi$ oscillates more quickly than $\cos^2\phi$ does as Fig. 6(e) suggests, however, that T_w^R remains small even in the presence of the $\cos^2\phi$ term. τ^{NR}, on the other hand, contains a component which does not vanish after the area integral. This property is inherited to the meridionally integrated wind stress torque

$$T_w^{NR} = \int T_w^{NR}(\phi)\, d\phi = \int\int_A \tau_\lambda^{NR} a \cos\phi\, dA,$$

even if the factor of $\cos\phi$ is multiplied. Thus, after the meridional integration, T_w^{NR} dominates T_w^R and most of T_w is contributed by T_w^{NR}. For non-rotational wind stress, shallow water gravity waves play a dominant role in accomplishing a balance between the wind stress and the pressure gradient force. Thus, $T_c^{NR}(\phi)$ is nearly equal to $T_w^{NR}(\phi)$, and therefore $T_c^{NR}(\phi)$ also has a component which does not vanish after the meridional integration.

In spite of the significant seasonally-varying amplitude of $T_w^R(\phi)$, the amplitude of $T_c^R(\phi)$ is small, and is less than that of T_b^R. This may be partly because the surface displacement associated with ocean circulations is large near the center of the oceans, but is less significant near the eastern and western boundaries. Both $T_c^R(\phi)$ and $T_b^R(\phi)$ become small after the meridional integration just as $T_w^R(\phi)$ does so.

Using an output of a rigid-lid version of the oceanic general circulation model (OGCM) by Semtner and Chervin (1992), Ponte and Rosen (1994) showed that the wind stress torque given at the sea surface is nearly balanced with the continental torque (Fig. 8 in their paper). In three-dimensional numerical models with density stratification such as the one used by Semtner and Chervin (1992), part of the surface pressure field is communicated to the bottom through the barotropic response, while the rest causes the baroclinic response which tends to reduce the horizontal pressure gradient at the bottom: the baroclinic response tends to achieve an isostacy in the steady state. If the pressure gradient given at the surface penetrates into the bottom through this baroclinic process, the torque exerted on the solid earth must be smaller than that due to the barotropic process. As far as the seasonal variation of the oceanic torque is concerned, the barotropic contribution is important even in the stratified ocean.

5.2. *Seasonal variation of oceanic torques*

It is important to note that the seasonal variations of the torques are caused by a very subtle balance among the torques at various latitudes. For example, let us compare Fig. 3 with Fig. 6(a) to find the role of the wind stress torque at different latitudes in producing the seasonal variation of the continental torque. The minimum in the wind stress torque in April (a in Fig. 3) corresponds to the weak wind stress regimes during the transient period from winter to summer in the Northern Hemisphere, and that from summer to winter in the Southern Hemisphere. The peak in June (b in Fig. 3) is created by the large wind stress in the middle latitudes of the Southern Hemisphere, and the peak in September (c in Fig. 3) by the large wind stress in the sub-tropical latitudes of the Northern Hemisphere. Figure 6(a) indicates that the complicated behavior of the seasonal variation of the wind stress torque is caused by the small phase shift of the seasonal change at different latitudes. Because of these characteristics, the relatively simple seasonal variation of the wind stress torque at each latitude does not lead to a simple seasonal variation of the continental torque.

Boer (1990) investigated the exchange of angular momentum between the atmosphere and the solid earth using output data of the atmospheric general circulation model of the Canadian Climate Centre. He calculated the torques given to the solid earth, the mountain torque and the wind stress torque at land and ocean surfaces. According to his result (Fig. 3 in his paper), a semiannual cycle of the total torque is dominant, because the angular momentum of the atmosphere is accumulated in winter in each Hemisphere. However, the oceanic torque has only a single minimum[6] in April. On the other hand, Fig. 3 in the present study shows one minimum in April and two maxima in June and September. The reason for the difference becomes evident when the latitudinal distribution of the seasonal cycle of his oceanic torque [his Fig. 6(e)] is compared with Fig. 6 in the present paper. His minimum in April is created by the same mechanism as the one in the present study. The two peaks in June and September in our result are created by the phase difference of the seasonal variation of the torque among different latitudes. However, the phase relationship in his study did not create extreme values except the one in April. The seasonal variation of the oceanic torque results from a delicate phase difference in the seasonal cycle at different latitudes as described above.

6. Conclusions

The physical mechanism that causes the seasonal variation of the angular momentum transfer from the atmosphere to the solid earth via the oceans is studied by means of a linear shallow-water numerical model of quasi-global oceans with no explicit surface Ekman boundary layer. A novel way to decompose the wind stress into rotational and non-rotational components is devised. Ocean circulations are caused solely

[6] His definition of the sign of the torque is opposite to ours. Therefore, our 'maximum' corresponds to his minimum and vice versa.

by the rotational wind stress, while the non-notational wind stress balances with the pressure gradient force caused by the surface elevation within a frame work of the barotropic shallow-water model. It is found that the seasonally-varying amplitude of the rotational wind stress torque at each latitudinal belt is larger than that of the non-rotational wind stress torque. However, once integrated with respect to latitude, the non-rotational wind stress torque dominates the rotational torque. The force relationship between the pressure and the wind stress, which strictly holds for ocean circulation on a beta plane in a steady state, remains essentially valid even for the seasonally varying real oceans for which the dependence of the arm length on latitude needs to be considered. As a result of these facts, most of the continental torque is caused by the non-rotational wind stress, and surprisingly little contribution to the continental torque is made by the ocean circulation which is driven by the rotational wind stress. The rapid transfer of the angular momentum via the oceans is realized because shallow water gravity waves are responsible for the adjustment between the non-rotational wind stress and the sea surface displacement.

7. Acknowledgments

We are grateful to Prof. A. Masuda, Research Institute for Applied Mechanics, Kyushu University, for allowing us to use the numerical codes of a β-plane version of his shallow water model, and to Prof. K. Iga, Research Institute for Applied Mechanics, Kyushu University, for suggesting the finite-difference scheme to conserve the angular momentum. Thanks are extended to Prof. T. Oki, Institute of Industrial Science, University of Tokyo for providing the Land and Ocean Distribution Data, and to Prof. I. Naito, Division of Earth Rotation, National Astronomical Observatory in Mizusawa, for introducing an interesting problem of the Earth Rotation and for giving helpful comments to us. Two anonymous reviewers contributed to improving the quality of the paper significantly. Support and encouragement by the members of the Marine Meteorology Division, Ocean Research Institute, and Geophysical and Planetary Physics Department, University of Tokyo, are greatly appreciated. This work was partly supported by a Grant-in-Aid for Scientific Research on Priority Area(B)(2) No.12125201, from the Ministry of Education, Culture, Sports, Science and Technology, Japan.

8. Appendix A: Angular momentum conservation in finite-difference equation and estimation of the surface displacement at the coast

The angular momentum of a fluid parcel of unit volume rotating about the polar axis is given by

$$m = m_\Omega + m_r = \rho\Omega a^2 \cos^2\phi + \rho u a \cos\phi, \tag{17}$$

where ρ is the density, and Ω is the earth's mean rotation rate (Gill, 1982). m_Ω is the planetary angular momentum due to solid-body rotation, and m_r the relative angular momentum due to zonal motions relative to the solid-body rotation. The time rate of change of M, the volume integral of m over the global ocean, is written as

$$\frac{dM}{dt} = \frac{d(M_\Omega + M_r)}{dt} = \frac{d}{dt}\int_V (m_\Omega + m_r)\, dV, \tag{18}$$

where M_Ω and M_r are volume integrals of m_Ω and m_r, respectively.

The time rate of change of M_r may be calculated from Eq. (8) as

$$\begin{aligned}\frac{dM_r}{dt} &= \frac{d}{dt}\int_V m_r\, dV = D\int_\phi\int_\lambda \rho\,\frac{\partial u}{\partial t}\cdot(a\cos\phi)\, dA\\ &= \rho D\int_\phi\int_\lambda fv\cdot(a\cos\phi)\, dA\\ &\quad - \rho Dg\int_\phi\int_\lambda \frac{\partial\eta}{\partial\lambda}\, dA + \int_\phi\int_\lambda \tau_x\cdot(a\cos\phi)\, dA\\ &\quad - \rho DR\int_\phi\int_\lambda u\cdot(a\cos\phi)\, dA.\end{aligned} \tag{19}$$

where $dA = a^2\cos\phi\, d\phi\, d\lambda$. The second, third and fourth terms on the right-hand side (RHS) of Eq. (19) are the continental torque T_c, the wind stress torque T_w and the bottom frictional torque T_b, respectively.

On the other hand, the time rate of change of M_Ω is calculated from Eq. (10) as

$$\frac{\mathrm{d}M_\Omega}{\mathrm{d}t} = \frac{\mathrm{d}}{\mathrm{d}t}\int_V m_\Omega \,\mathrm{d}V$$
$$= \int_\phi \int_\lambda \rho\Omega \frac{\partial \eta}{\partial t} \cdot (a^2 \cos^2 \phi)\,\mathrm{d}A$$
$$= -\rho\Omega a D \int_\phi \int_\lambda \frac{\partial u}{\partial \lambda} \cos\phi \,\mathrm{d}A$$
$$-\rho\Omega a D \int_\phi \int_\lambda \frac{\partial (v\cos\phi)}{\partial \phi} \cos\phi\,\mathrm{d}A. \quad (20)$$

The addition of Eq. (19) to Eq. (20) gives Eq. (11) after some manipulation, which states that the total oceanic angular momentum M is conserved (Gill, 1982; Ponte, 1990). The first purpose of this appendix is to show that this angular momentum conservation is in fact satisfied by our finite-difference numerical model.

In the present numerical simulation, the basic shallow water equations (8) and (10) in the finite-difference form are written as:

$$\frac{\partial u_{i,j}}{\partial t} = -\frac{f}{4\cos\phi_j}[\cos\phi_{j+1/2}(v_{i,j} + v_{i+1,j})$$
$$+ \cos\phi_{j-1/2}(v_{i,j-1} + v_{i+1,j-1})]$$
$$-\frac{g}{a\cos\phi_j}\frac{\eta_{i+1,j} - \eta_{i,j}}{\Delta\lambda} + \frac{\tau_{\lambda i,j}}{D\rho} - Ru_{i,j}, \quad (21)$$

$$\frac{\partial \eta_{i,j}}{\partial t} = -D\frac{1}{a\cos\phi_j}\left(\frac{u_{i,j} - u_{i-1,j}}{\Delta\lambda}\right.$$
$$\left. + \frac{v_{i,j}\cos\phi_{j+1/2} - v_{i,j-1}\cos\phi_{j-1/2}}{\Delta\phi}\right). \quad (22)$$

where f_j and ϕ_j are evaluated at the latitude of $\eta_{i,j}$, and $\cos\phi_{j+1/2}$ at the latitude of $v_{i,j}$ (Fig. 1). $\Delta\lambda$ and $\Delta\phi$ are longitudinal and latitudinal grid intervals, respectively. The intriguing factors like $\cos\phi_{j+1/2}/\cos\phi_j$ and $\cos\phi_{j-1/2}/\cos\phi_j$ in Eq. (21) enable the system to conserve the total angular momentum as will be shown below.

Now, let us first consider the finite-difference representation of Eq. (18) based on the volume integral of Eq. (21). Let i and j be the zonal and meridional grid numbers. i varies from I_w to I_e and j from J_s to J_n, respectively, where I_w, I_e, J_s and J_n are the grid numbers at the western, eastern, southern and northern coasts, respectively. Since no normal flow exists at the boundaries,

$$u_{I_w,j} = u_{I_e-1,j} = 0 \quad (23)$$

and

$$v_{i,J_s} = v_{i,J_n-1} = 0. \quad (24)$$

The first term on the RHS of Eq. (19) is

$$\rho D a^3 \int_\phi \int_\lambda f v \cos^2\phi \,\mathrm{d}\phi\,\mathrm{d}\lambda$$
$$= -\rho D a^3 \Omega\,\Delta\lambda$$
$$\times \sum_{j=J_s+1}^{J_n-1} \sum_{i=I_w+1}^{I_e-1} \frac{\cos^2\phi_{j+1/2} - \cos^2\phi_{j-1/2}}{2}$$
$$\times (v_{i,j}\cos\phi_{j+1/2} + v_{i,j-1}\cos\phi_{j-1/2}), \quad (25)$$

where the free slip conditions $v_{I_w,j} = v_{I_w+1,j}$ and $v_{I_e-1,j} = v_{I_e,j}$, at the east and west boundaries, respectively, have been used, and the Coriolis parameter

$$f_j = 2\Omega\sin\ \phi = -\frac{\Omega}{\cos\phi}\frac{\mathrm{d}}{\mathrm{d}\phi}(\cos^2\phi)$$

is evaluated as

$$f_j \equiv -\Omega\frac{\cos^2\phi_{j+1/2} - \cos^2\phi_{j-1/2}}{\Delta\phi\cos\phi_j}. \quad (26)$$

Egger and Hoinka (1999) independently invented the same finite-difference representation of the Coriolis parameter that is essential to the conservation of angular momentum.

The first term on the RHS of Eq. (20) is rewritten in the finite-difference representation as

$$-\rho D a^3 \Omega\,\Delta\phi \sum_{j=J_s+1}^{J_n-1} \cos^2\phi \sum_{i=I_w+1}^{I_e-1} \Delta u$$
$$= -\rho D a^3 \Omega\,\Delta\phi \sum_{j=J_s+1}^{J_n-1} \frac{\cos^2\phi_{j+1/2} + \cos^2\phi_{j-1/2}}{2}$$
$$\times (u_{I_e-1,j} - u_{Iw,j}), \quad (27)$$

which vanishes because of Eq. (23).

The second term on the RHS of Eq. (20) is given by

$$-\rho D a^3 \Omega\, \Delta\lambda \times \sum_{j=J_s+1}^{J_n-1} \sum_{i=I_w+1}^{I_e-1} \frac{\cos^2\phi_{j+1/2} + \cos^2\phi_{j-1/2}}{2} \times (v_{i,j}\cos\phi_{j+1/2} - v_{i,j-1}\cos\phi_{j-1/2}). \quad (28)$$

Adding Eq. (28) to Eq. (25), we obtain

$$-\rho D a^3 \Omega\, \Delta\lambda \sum_{i=I_w+1}^{I_e-1} (v_{i,J_n-1}\cos^3\phi_{J_n-1/2} - v_{i,J_s} \times \cos^3\phi_{J_s+1/2}), \quad (29)$$

which vanishes because of Eq. (24). Thus, the present numerical scheme exactly conserves the angular momentum.

The continental torque is calculated from the second term on the RHS of Eq. (19) as

$$\rho D g a^2\, \Delta\phi \sum_{j=J_s+1}^{J_n-1} \cos\phi \sum_{i=I_w+1}^{I_e-1} \Delta\eta = \rho D g a^2\, \Delta\phi \times \sum_{j=J_s+1}^{J_n-1} \left(\frac{\eta_{I_e-1/2,j} + \eta_{I_e-1,j}}{2} - \frac{\eta_{I_w+1,j} + \eta_{I_w+1/2,j}}{2} \right) \cos\phi_j. \quad (30)$$

It is caused by the pressure difference at the eastern and western boundaries.

At the western boundary, Eq. (8) together with the boundary condition $u = 0$ and $\tau_\lambda = 0$ gives

$$fv = \frac{g}{a\cos\phi}\frac{\partial\eta}{\partial\lambda}. \quad (31)$$

The finite-difference representation of this equation that conserves the angular momentum is

$$-\frac{f_j}{4}[\cos\phi_{j+1/2}(v_{I_w,j} + v_{I_w+1,j}) + \cos\phi_{j-1/2}(v_{I_w,j-1} + v_{I_w+1,j-1})] = \frac{g(\eta_{I_w+1,j} - \eta_{I_w+1/2,j})}{a\Delta\lambda/2}, \quad (32)$$

[see Eq. (21)]. Using the free-slip boundary conditions $v_{I_w,j} = v_{I_w+1,j}$ and $v_{I_w,j-1} = v_{I_w+1,j-1}$, we obtain

$$\eta_{I_w+1/2,j} = \eta_{I_w+1,j} - \frac{f_j}{g} \times \frac{v_{I_w+1,j}\cos\phi_{j+1/2} + v_{I_w+1,j-1}\cos\phi_{j-1/2}}{2} \times \frac{a\Delta\lambda}{2}. \quad (33)$$

Similarly, at the eastern boundary, we have

$$\eta_{I_e-1/2,j} = \eta_{I_e-1,j} + \frac{f_j}{g} \times \frac{v_{I_e-1,j}\cos\phi_{j+1/2} + v_{I_e-1,j-1}\cos\phi_{j-1/2}}{2} \times \frac{a\Delta\lambda}{2}. \quad (34)$$

The continental torque is obtained by substituting these relationship into Eq. (30). With the choice of $R^{-1} = 5$ d, the width of the Stommel boundary layer ($= R/\beta$, where $\beta = \mathrm{d}f/a\,\mathrm{d}\phi$ is the meridional derivative of the Coriolis parameter) is approximately 200 km (2°). This means that the width of the western boundary current is comparable to one grid interval in our model. It should be noted from Eq. (31), however, that the surface displacement at the coast is determined by the volume flow rate but not directly by the velocity profile. Thus, as far as the wind-driven circulation outside the western boundary layer is well resolved, the surface displacement at the western coast from Eq. (31) should be estimated within the accuracy of $O(\Delta\lambda/l)$, where l is the zonal width of the ocean.

9. Appendix B: Decomposition of wind stress into rotational and non-rotational components

Let us introduce functions $\Psi_\tau(\lambda, \phi)$ and $\Phi_\tau(\lambda, \phi)$ in the spherical coordinate, so that

$$\boldsymbol{\tau}(\lambda, \phi) = \nabla \times \Psi_\tau(\lambda, \phi) + \nabla\Phi_\tau(\lambda, \phi), \quad (35)$$

where $\boldsymbol{\tau}$ is the total wind stress. The first term on the RHS expresses the rotational component and the second term the non-rotational component.

To obtain the rotational wind stress, we take curl of Eq. (35):

$$\nabla^2\Psi_\tau(\lambda, \phi) = \frac{1}{a\cos\phi}\left(\frac{\partial\tau_\phi}{\partial\lambda} - \frac{\partial(\tau_\lambda\cos\phi)}{\partial\phi}\right). \quad (36)$$

The boundary condition is

$$\Psi_\tau(\lambda, \phi) = 0 \quad \text{along the coasts.} \tag{37}$$

$\Psi_\tau(\lambda, \phi)$ is obtained by solving numerically Eqs. (36) and (37) using the over-relaxation method. Once $\Psi_\tau(\lambda, \phi)$ is obtained, the rotational wind stress is calculated as

$$\boldsymbol{\tau}^{\mathrm{R}}(\lambda, \phi) = \left(-\frac{1}{a}\frac{\partial \Psi_\tau}{\partial \phi}, \frac{1}{a\cos\phi}\frac{\partial \Psi_\tau}{\partial \lambda} \right). \tag{38}$$

The non-rotational wind stress is obtained by

$$\boldsymbol{\tau}^{\mathrm{NR}}(\lambda, \phi) = \boldsymbol{\tau}(\lambda, \phi) - \boldsymbol{\tau}^{\mathrm{R}}(\lambda, \phi) \tag{39}$$

This calculation has been applied to the observed wind stress $\boldsymbol{\tau}$ by Hellerman and Rosenstein (1983).

REFERENCES

Boer, G. J. 1990. Earth–atmosphere exchanges of angular momentum simulated in a general circulation model and implications for the length of day. *J. Geophys. Res.* **95, D5**, 5511–5531.

Bryan, F. O. 1997. The axial angular momentum balance of a global ocean general circulation model *Dyn. Atmos. Oceans* **25**, 191–216.

Egger, J. and Hoinka, K.-P. 1999. The equatorial bulge, angular momentum and planetary wave motion. *Tellus* **51A**, 914–921.

Gill, A. E. 1982. *Atmosphere–ocean dynamics*. Academic Press, San Diego, CA, 662 pp.

Hellerman, S. and Rosenstein, M, 1983. Normal monthly wind stress over the world ocean with error estimates. *J. Phys. Oceanogr.* **13**, 1093–1104.

Ichikawa, H. and Beardsley, R. C. 1993. Temporal and spatial variability of volume transport of the Kuroshio in the East China Sea. *Deep Sea Res. Part I* **40**, 583–605.

Masuda, A. 1991. Oceanography and mathematics. *Sea and Sky* **67**, 163–175 (in Japanese).

Munk, W. H. and MacDonald, G. F. 1960. *The rotation of the earth*. Cambridge University Press, Cambridge, 323 pp.

Oort, A. H. 1985. Balance conditions in the earth's climate system, *Adv. Geophys.* **28A**, 75–98.

Oort, A. H. 1989. Angular momentum cycle in the atmosphere–ocean–solid earth system. *Bull. Am. Meteorol. Soc.* **70**, 1231–1242.

Oort, A. H. and Peixoto, J. P. 1992. *Physics of climate*. American Institute of Physics, Washington, DC, 520 pp.

Pedlosky, J. 1968. An overlooked aspect of the wind-driven oceanic circulation. *J. Fluid. Mech.* **32**, 809–821.

Ponte, R. M. 1990. Barotropic motions and exchange of angular momentum between the oceans and solid earth, *J. Geophys. Res.* **95, C7**, 11 369–11 374.

Ponte, R. M. and Gutzler, D. S. 1991. The Madden–Julian oscillation and the angular momentum balance in a barotropic ocean model. **96, C1**, 835–842.

Ponte, R. M. and Rosen, R. D. 1993. Determining torques over the ocean and their role in the planetary momentum budget. *J. Geophys. Res.* **98, D4**, 7317–7325.

Ponte, R. M. and Rosen, R. D. 1994. Oceanic angular momentum and torques in a general circulation model. *J. Phys. Oceanogr.* **24**, 1966–1977.

Rosen, R. D., Salstein, D. A. and Wood, T. M. 1990. Discrepancies in the earth-atmosphere angular momentum budget. *J. Geophys. Res.* **95**, 265–279.

Semtner, A. J. Jr and Chervin, R. M. 1992. Ocean general circulation from a global eddy-resolving model. *J. Geophys. Res.* **97, C4**, 5493–5550.

Stommel, H. 1948. The westward intensification of wind––driven currents, *Trans. Am. Geophys. Union* **29**, 202–206.

Veronis, G. 1996. Effect of a constant, zonal wind on wind-driven ocean circulation. *J. Phys. Oceanogr.* **26**, 2525–2538.

Wahr, J. M. and Oort, A. H. 1984. Friction- and mountain-torque estimates from global atmospheric data. *J. Atmos. Sci.* **41**, 190–204.